Available online at www.sciencedirect.com

SCIENCE DIRECT®

Biochimica et Biophysica Acta 1605 (2003) 35–46

BIOCHIMICA ET BIOPHYSICA ACTA

BBA

www.bba-direct.com

Hyperfine structure of the photoexcited triplet state ^{3}P680 in plant PS II reaction centres as determined by pulse ENDOR spectroscopy

Friedhelm Lendzian[a,*], Robert Bittl[b], Alison Telfer[c], Wolfgang Lubitz[d]

[a] *Max-Volmer-Laboratorium für Biophysikalische Chemie, Technische Universität Berlin, PC14, Strasse des 17. Juni 135, D-10623 Berlin, Germany*
[b] *Institut für Experimentalphysik, Freie Universität Berlin, Arnimalle 14, D-14195 Berlin, Germany*
[c] *Wolfson Laboratories, Department of Biological Sciences, Imperial College of Science, Technology and Medicine, London SW7 2AY, UK*
[d] *Max-Planck-Institut für Strahlenchemie, Stiftstrasse 34-36, D-45470 Mülheim/Ruhr, Germany*

Received 6 January 2003; received in revised form 28 May 2003; accepted 11 June 2003

Abstract

The triplet states in plant photosystem II (PS II), ^{3}P680, and from chlorophyll *a*, ^{3}Chl *a*, in organic solution have been investigated using pulse ENDOR combined with repetitive laser excitation at cryogenic temperature with the aim to obtain their hyperfine (hf) structure. The large zero field splitting (ZFS) tensor of ^{3}P680 enabled orientation selection via the electron spin resonance (EPR) field setting along the ZFS tensor axes. ENDOR spectra have been obtained for the first time also for the in-plane *X*- and *Y*-orientations of the ZFS tensor. This allowed a full determination of the hf-tensors of the three methine protons and one methyl group of ^{3}P680. Based on the orientations of the axes of these hf-tensors, a unique orientation of the axes of the ZFS tensor of ^{3}P680 in the Chl *a* molecular frame was obtained. These data serve as a structural basis for determining the orientation of ^{3}P680 in the PS II protein complex by EPR on single crystals (see M. Kammel et al. in this issue). The data obtained represent the first complete set of the larger hf-tensors of the triplet state ^{3}P680. They reflect the spin density distribution both in the highest occupied (HOMO) and lowest unoccupied (LUMO) orbitals. The data clearly confirm that ^{3}P680 is a monomeric Chl *a* species at low temperature (T = 10 K) used, as has been proposed earlier based on *D*- and *E*-values obtained from EPR and optically detected magnetic resonance (ODMR) studies. Comparison with the hf data for the cation and anion radicals of Chl *a* indicates a redistribution of spin densities in particular for the LUMO orbital of the triplet states. The electron spin distribution in the LUMO orbital is of special interest since it harbours the excited electron in the excited P680 singlet state, from which light-induced electron transfer proceeds. Observed shifts of hf couplings from individual nuclei of ^{3}P680 as compared with ^{3}Chl *a* in organic solution are of special interest, since they indicate specific protein interactions, e.g. hydrogen bonding, which might be used in future studies for assigning ^{3}P680 to a particular chlorophyll molecule in PS II.

Keywords: Photosystem II; Primary donor; P680; Triplet state; Chlorophyll; ENDOR

1. Introduction

In reaction centres (RCs) of photosynthetic organisms, charge separation starts from the photoexcited singlet state of a chlorophyll (Chl) or bacteriochlorophyll (BChl) species, called the primary donor P, and proceeds via a series of chlorophyll, pheophytin (Ph) and quinone (Q) acceptors, which finally leads to a potential difference across the photosynthetic membrane that drives the following dark reactions [1]. Type I RCs (plant photosystem I and green bacteria) [2–4] contain (B)Chl as intermediate and secondary electron acceptors followed by a quinone (vitamin K1) and three iron–sulfur centres. Type II RCs (purple bacterial and plant photosystem II) [3–6] contain (bacterio)pheophytin (BPh) as secondary acceptor followed by two quinone acceptors, Q_A and Q_B, which are in close contact to a non-heme iron centre. The transient radical cation and anion states of almost all molecules of this electron transfer (ET) chain have been characterised in terms of their electronic structure and interaction with the protein in great

Abbreviations: EPR, electron spin resonance; ENDOR, electron nuclear double resonance; HF, hyperfine; PS II, plant photosystem II; ^{3}P680, triplet state observed by charge recombination in PS II; ^{3}Chl *a*, triplet state of chlorophyll *a* obtained from intersystem crossing; ZFS, zero field splitting; *D* and *E*, parameters describing the zero field splitting in triplet states

* Corresponding authors. F. Lendzian is to be contacted at Tel.: +49-30-314-22489; fax: +49-30-314-21122. W. Lubitz is to be contacted at Tel.: +49-208-306-3614; fax: +49-208-306-3955.

E-mail addresses: lendzian@struktur.chem.tu-berlin.de (F. Lendzian), lubitz@mpi-muelheim.mpg.de (W. Lubitz).

0005-2728/03/$ - see front matter © 2003 Elsevier B.V. All rights reserved.
doi:10.1016/S0005-2728(03)00062-8

detail by a variety of electron spin resonance (EPR) techniques [7–11].

Under physiological conditions, triplet states of the chlorophyll or pheophytin molecules are not observed in the RCs. Chlorophyll triplet states are carefully avoided, since they lead, in the presence of oxygen, via triplet–triplet quenching to formation of singlet oxygen, which in turn leads to cell damage. This is prevented by incorporation of carotenoid molecules in all photosystems, which effectively quench the chlorophyll triplet states, resulting from intersystem crossing, by fast triplet energy transfer. The carotenoid triplet state is too low in energy to enable formation of singlet oxygen and is deactivated by internal conversion to the singlet ground state [12]. However, when the electron transport to the quinone acceptors is blocked by pre-reduction, coherent singlet–triplet mixing in the primary radical ion pair leads to recombination and formation of the triplet state of the primary donor, ^{3}P, which is formed (in particular at low temperatures) with high yield [13].

Although ^{3}P is not a functional state during normal electron transfer, its investigation is important for several reasons. (i) Using time-resolved spectroscopy, kinetic studies were performed in order to determine the important triplet energy transfer rates [13–16]. (ii) For understanding the triplet state ^{3}P and its reactions, its electronic structure is of considerable interest [14]. (iii) Formation of ^{3}P680 has been implicated in photoinhibition, a physiologically significant phenomenon, which at high light intensities leads to a decrease in plant productivity [17]. (iv) ^{3}P exhibits two unpaired electrons, one in the highest occupied molecular orbital (HOMO), the other in the lowest unoccupied molecular orbital (LUMO). The spatial distribution of the LUMO is of particular interest since charge separation occurs from this orbital in the excited singlet state. Since the excited singlet state is short-lived and diamagnetic, information on the electronic distribution of the LUMO is only available via the triplet state [14,18].

The two interacting unpaired electrons in the HOMO and LUMO in ^{3}P lead to a zero field splitting (ZFS) in the spectra, described by two parameters, D and E, which have been investigated in great detail by optical detected magnetic resonance (ODMR) [8,13,19] and EPR techniques [14,19,20]. For the bacterial RC the obtained D- and E-values indicated that ^{3}P is delocalized over the two BChl a molecules which constitute P. In plant PS I (^{3}P700) and II (^{3}P680) the D- and E-values indicate a localization of the triplet state on one Chl a molecule at low temperature [8,13,14,20,21]. Interestingly, a similar behaviour was found for the respective cation radical states $P^{+\bullet}$ based on their hyperfine (hf) data obtained from electron nuclear double resonance (ENDOR) spectroscopy [9,11,22–27]. The localisation of the triplet states is in contrast to the respective excited singlet states ^{1}P700 and ^{1}P680, which are known to be excitonically delocalized [28,29]. While excited singlet states interact via excitonic coupling (Förster mechanism) [30] over large distances, excited triplet states interact via the Dexter mechanism, which requires orbital overlap and hence much closer distances [31].

The ZFS parameters D and E, on which most of the interpretations were so far based, are integral properties of the triplet wave function, and depend on its overall spatial distribution. However, electronic properties, in particular the amount of charge transfer character in a dimeric species, strongly affect the observed D- and E-values [14,18]. This seriously complicates their interpretation. Additional and more specific information about the electron distribution in the HOMO and LUMO orbitals is obtained from the electron-nuclear hyperfine couplings (hfc), from which the distribution of the unpaired electrons of ^{3}P is obtained. In contrast to the large body of EPR and ODMR investigations, yielding D- and E-values, there are only a few studies on the hf structure of the triplet state ^{3}P, which is only resolved by ENDOR spectroscopy [18,32,33]. Pulse ENDOR combined with repetitive laser excitation at low temperatures is well-suited since this method takes advantage of the large spin polarization of ^{3}P being present only in the first few microseconds after the laser pulse. In an earlier pulse ENDOR study on ^{3}P865 in RCs of the bacterium *Rhodobacter sphaeroides*, we could show that by this method hf-tensor components including their signs (relative to that of D) can be obtained, which enabled an assignment to specific nuclei and, by comparison with the cation and anion radical of BChl a, allowed us to discriminate between hf couplings from the HOMO and LUMO orbitals. Thereby a detailed characterization of ^{3}P865 was obtained showing an asymmetric distribution of this triplet state over the two BChl a molecules constituting ^{3}P865. In a dimeric species (P_LP_M, where L and M indicate the two branches of pigments), a delocalized triplet state is a superposition of four contributions [18]. The two local excitations, $^3P_LP_M$ and $P_L^3P_M$, and the two charge transfer states, $^3(P_L^{+\bullet}P_M^{-\bullet})$ and $^3(PL^{-\bullet}P_M^{+\bullet})$. Our data indicated for ^{3}P865 a significant charge transfer character ($\approx$ 20%), most probably in favour of $^3(P_L^{+\bullet}P_M^{-\bullet})$ [18].

The primary donor, P680, of plant PS II is of particular interest for several reasons. The origin of the strongly positive oxidation midpoint potential for P680/P680$^{+\bullet}$ ($\geq$ 1.2 V), necessary for water splitting, is still not understood. It indicates unusual orbital energies, most probably induced by interactions with the protein, that change the electronic properties as compared with Chl a in organic solvents. ENDOR investigations have been performed to explore the hf structure of the cation radical P680$^{+\bullet}$. No dramatic changes have been found as compared with Chl $a^{+\bullet}$ in organic solvents or the cation radical of Chl_z, which acts as donor to P680$^{+\bullet}$ in plant PS II [26,27]. However, these studies have also shown that it is not possible to accumulate P680$^{+\bullet}$ with low temperature illumination in the presence of external donors, without having contributions from $Chl_z^{+\bullet}$ and/or other Chl$^{+\bullet}$ species. Furthermore, depending on the conditions, also additional carotenoid cation radicals were observed [26,27,34,35].

The triplet state in PS II, ^{3}P680, is easier to prepare. Interactions with the protein are expected to influence its hf structure, which reflects the spin density distributions both in the HOMO and LUMO orbital. It is however important to note that unlike in bacterial RCs the triplet state, ^{3}P680 may reside on a molecule different from the cation radical state $P680^{+\bullet}$. A localization of ^{3}P680 on one of the accessory chlorophylls, Chl_{D1} or Chl_{D2}, was suggested earlier by van Mieghem et al. [36], based on EPR investigations on oriented plant PS II membrane fragments. Recent EPR work on PS II single crystals corroborates this suggestion and yields additional details on the triplet axes [37]. Interestingly, models for the light-induced charge separation in PS II have been discussed, which are different from those for bRCs and involve Chl_{D1} as early primary donor, before the positive charge moves on to P680 [38–40].

In this paper we report on a pulse ENDOR investigation of ^{3}P680 in PSII RCs (also known as the D1D2 cytochrome *b*559 complex) and the triplet state of isolated chlorophyll, ^{3}Chl *a*, in frozen organic solvents, using repetitive laser excitation. The large ZFS enabled single crystal type ENDOR spectra to be recorded, using the EPR field position for selection of molecules with particular orientations in the frozen solution samples for the ENDOR experiment. This study gives the first complete picture of the large hf-tensors, which are important to characterize the unpaired electron distribution in the two triplet states ^{3}P680 and ^{3}Chl *a*. The anisotropic hf-tensor components presented here, for all three canonical orientations of the triplet state, enable an assignment to specific nuclei and thereby allow a determination of the orientation of all three triplet axes, with respect to the molecular axes of ^{3}P680. This result is a prerequisite for the interpretation of the EPR data obtained for ^{3}P680 in PS II single crystals [37]. Comparison of the hf data with those of ^{3}Chl *a* in organic solvents clearly confirms that ^{3}P680 is a monomeric chlorophyll triplet species at $T=10$ K. Observed shifts of individual hf couplings different from those in organic solvents indicate specific interactions with the protein.

2. Materials and methods

2.1. Sample preparation

Chl *a* was extracted from spinach and dissolved in highly purified deoxygenated 2-methyl tetrahydrofuran (MTHF). Samples (concentration ≈ 1 mM) were prepared anaerobically on a high vacuum line in standard EPR quartz tubes (4-mm O.D., 3-mm I.D.), sealed and then quickly frozen in liquid nitrogen to form an optically transparent glass. PS II RCs (D1/D2-cyt *b*-559) lacking the quinone acceptors were prepared from pea as described previously [41,42] and concentrated to ≈ 0.5 mM. Triplet states were generated inside the optically transparent dielectric ring ENDOR resonator (Bruker, ESP 380-1052 DLQ-H) at $T=10$ K using repetitive pulse laser excitation; see below [18].

2.2. Transient and pulse EPR

Transient EPR was performed using continuous microwave irradiation and recording transient signals after laser pulse excitation for each field position. The spectrum was obtained by plotting the integrated signal intensity between 0.5 and 1.5 μs versus the magnetic field (Ref. [43], see accompanying paper).

Pulse EPR spectra were recorded using a pulse sequence as outlined in Fig. 1, leaving out the rf pulse. Spectra were obtained by plotting the integrated echo intensity as function of the magnetic field.

2.3. Pulse ENDOR

Pulse ENDOR experiments were performed on a Bruker ESP 380E pulse EPR spectrometer equipped with a Bruker ESP 360D-P pulse ENDOR accessory, a 500-W ENI A500 radio frequency amplifier, and an Oxford CF935 cryostat for temperature control. Samples were excited inside the optically transparent dielectric ring ENDOR resonator with a frequency doubled Nd:YAG laser (Spectra-Physics, GCR 130) with 8-ns pulses at 532 nm and ~ 10-mJ incident light energy per pulse with a 10-Hz repetition rate. According to the Davies ENDOR scheme [44], weak selective microwave pulses synchronized with the laser pulses were used for preparation (first π pulse 1 μs after the laser pulse) and for detection (echo sequence π/2, π, ~ 3 μs after the end of the radio frequency π pulse (Fig. 1). The 56- and 112-ns microwave π/2 and π pulses correspond to a rotating frame microwave field strength of $B_1 \approx 0.16$ mT. The 8-μs RF pulse with an rf field strength of $B_2 \approx 1.5$ mT is a π pulse for protons. A comprehensive description of pulse EPR and ENDOR techniques has been given by Schweiger [44]. Pulse ENDOR spectra were accumulated for ≈ 15 h at 10 K.

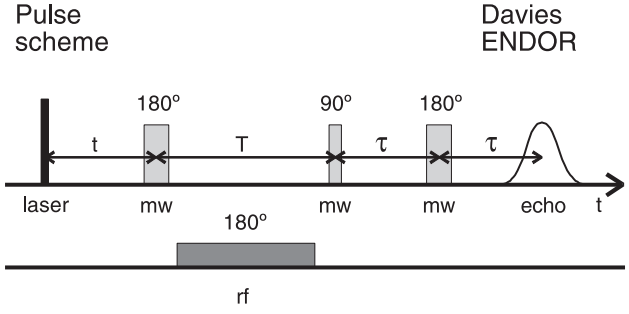

Fig. 1. Pulse scheme for Davies ENDOR on photoexcited triplet states of ^{3}Chl *a* and ^{3}P680 showing laser, microwave (mw) and radio frequency (rf) ENDOR pulses. $t=1$ μs, $T=12$ μs, $\tau=250$ ns; pulse durations: laser: 8 ns, mw 90° pulse: 56 ns, mw 180° pulse: 112 ns, rf 180° pulse: 8 μs. For other conditions see text.

3. Results

3.1. EPR spectra

Fig. 2A shows the Zeeman splitting of the spin energy levels for the three canonical orientations of a triplet state (magnetic field parallel to the triplet axes *X*, *Y*, and *Z*) for the case of a zero-field splitting parameter $D>0$. For ^{3}P680 a positive sign of *D* is expected, as it is generally the case for $\pi-\pi^*$ triplet states of porphyrins [36]. ^{3}P680 is formed by charge recombination from the singlet-born primary radical pair $P^{+\bullet}Ph^{-\bullet}$. This leads in a magnetic field to exclusive population of the $m_S=0$ sublevel, as indicated by bold lines (Fig. 2A) [8,13,14]. From this scheme the spin polarization pattern in the EPR spectrum is expected to be AEEAAE (A = absorption, E = emission), proceeding from the low-field Z_I, via X_{II},... to Z_{II} at the high-field side. The possible EPR transitions for the three canonical orientations are indicated in Fig. 2A. The transient EPR spectrum of ^{3}P680 obtained in frozen PSII RC solution at 10 K is shown in Fig. 2B. The spectrum exhibits the predicted polarization pattern from Fig. 2A. The dotted traces show the simulated powder pattern (sum of all possible orientations) for the $m_S=0$ to $m_S=+1$ transition (X_I, Y_I, Z_I), in absorption, and for the $m_S=0$ to $m_S=-1$ transition, (X_{II}, Y_{II}, Z_{II}), in emission. The observed spectrum is the superposition of both patterns.

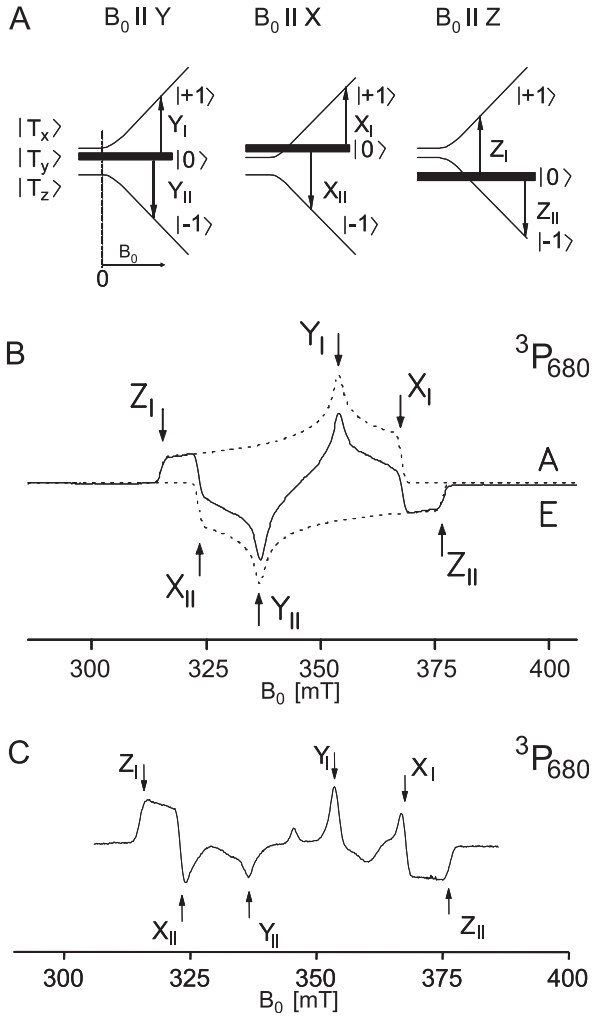

Fig. 2. (A) Electron spin energy levels of a triplet state with D>0 for the canonical orientations (field parallel to the ZFS tensor axes, *X*, *Y*, *Z*, as function of the magnetic field (see text). (B) Transient EPR spectrum of ^{3}P680 at $T=10$ K. Dotted traces: Simulated powder pattern for the $m_S=0$ to $m_S=1$ transitions (absorption, index I) and the $m_S=0$ to $m_S=-1$ transitions (emission, index II). (C) Field-swept ESE spectrum (integrated echo intensity as function of the field) of ^{3}P680 at $T=10$ K, showing diminished signal intensities for noncanonical orientations. Pulse parameters were the same as given in Fig. 1, except that the rf pulse was omitted.

In contrast to ^{3}P680 the triplet state of Chl *a* in MTHF is generated by spin–orbit-coupling-induced intersystem crossing from the photoexcited singlet state of Chl *a*. This process leads to a lower triplet yield as compared with ^{3}P680 and also to a lower spin polarisation since more than one triplet sublevel is occupied [14]. The observed polarisation pattern is EAEAEA, starting with the low field Z_I transition (spectrum not shown).

The zero-field splitting parameters obtained for ^{3}P680 were $|D|=287\times10^{-4}$ cm^{-1} ± 1% and $|E|=43\times10^{-4}$ cm^{-1} ± 8%. For the triplet of ^{3}Chl *a* in MTHF (spectrum not shown) we obtained $|D|=282\times10^{-4}$ cm^{-1} and $|E|=38\times10^{-4}$ cm^{-1} with similar errors. The values for both triplet states agree within their error margins and are in good agreement with values reported earlier for both triplet states [13,14,21]. This is in contrast to the case of ^{3}P865 in the bacterial RCs, where a strong reduction (ca 30%) of both the *D*- and *E*-values as compared with those of ^{3}BChl *a* in organic solvent was observed, which was attributed to delocalization of the triplet state over two BChl *a* molecules in ^{3}P865 [13,14,20].

Fig. 2C shows the field-swept electron spin echo (ESE) spectrum of ^{3}P680 also obtained at $T=10$ K. The spectrum was recorded with the same microwave pulse parameters as used for the ENDOR spectra, except for the missing rf pulse (see below). Comparison with the transient EPR spectrum (Fig. 2B) clearly shows that in the pulse EPR spectrum the intensities of noncanonical orientations (field positions in between the *X*-, *Y*-, and *Z*-orientations are diminished (see discussion below).

3.2. Pulse ENDOR spectra

3.2.1. ENDOR spectra from the Z_I- and Z_{II}-orientations

Pulse ENDOR spectra of ^{3}P680 and ^{3}Chl *a* were recorded starting with field settings corresponding to the respective Z_I and Z_{II} EPR transitions (Fig. 3B). Thereby exclusively orientations of ^{3}P680 and ^{3}Chl *a* molecules with their respective triplet z axis, *Z*, parallel to B_0 were selected, yielding single crystal-like ENDOR spectra. Fig. 3A shows the spin energy levels for this specific case, including hf interaction for one nuclear spin $I=1/2$ in the high-field limit [46]. The Z_I and Z_{II} EPR transitions are indicated by thin

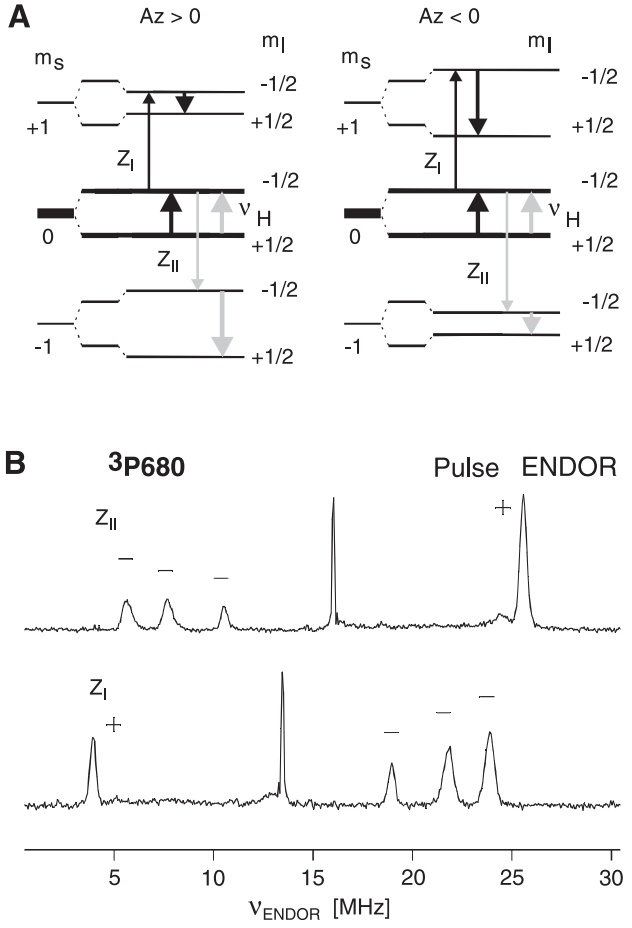

Fig. 3. (A) Spin energy levels of a triplet state showing positive and negative hyperfine splitting A_Z from one nucleus with spin $I=1/2$ for the field parallel to the Z-axis of the ZFS tensor. Black thin arrows: $m_S=0$ to $m_S=1$ EPR transition (Z_I); black thick arrows: ENDOR transitions for Z_I. Gray thin arrows: $m_S=0$ to $m_S=-1$ EPR transition (Z_{II}); gray thick arrows: ENDOR transitions for Z_{II}. (B) Pulse ENDOR spectrum of ^{3}P680 for the Z_I and Z_{II} EPR field positions (compare Fig. 2). Note that the two ENDOR spectra are shifted (see shift of the intense narrow line at ν_H) due to the large difference between the two field positions.

black and grey arrows, the ENDOR transitions by bold black arrows (Z_I field position) and bold grey arrows (Z_{II} field position). From this scheme, it is clear that the ENDOR transition frequencies are no longer symmetrically spaced about the nuclear Zeeman frequency, ν_H, as for a doublet state ($S=1/2$). Instead, a strong line is expected from the $m_S=0$ manifold at the Larmor frequency, ν_H, and for the EPR Z_I transition (connecting the $m_S=0$ and $m_S=+1$ levels), one hf shifted ENDOR line is expected at $\nu_H-A_Z(i)$ for each nucleus i. In case of $A_Z(i)>0$ this line occurs on the low-frequency side, in case of $A_Z(i)<0$ on the high-frequency side with respect to ν_H. When the EPR Z_{II} transition, connecting the $m_S=0$ and $m_S=-1$ levels, is driven with the microwave π-pulse, the lines change sides in the ENDOR spectrum (Fig. 3). Hence, the magnitude and the sign of the hf coupling $A_Z(i)$ (relative to the sign of D) are directly obtained from the shift of the respective ENDOR line relative to ν_H. Note that $A_Z(i)$ is the hf tensor component along the triplet Z-axis, which is perpendicular to the π-plane. Furthermore, the ENDOR spectrum connected with the $m_S=0$ to $m_S=+1$ EPR transition (Z_I) is expected to be in absorption, while that connected with the $m_S=0$ to $m_S=-1$ EPR transition (Z_{II}) should be in emission [26].

The pulse ENDOR spectra of ^{3}P680 at $T=10$ K for the Z_I and Z_{II} EPR transition show indeed the expected behaviour (Fig. 3B). A strong, narrow line is observed at ν_H and, in addition, four broader lines are observed, one shifted to higher and three to lower frequencies. According to Fig. 3A, the low-frequency ENDOR line in the spectrum for the Z_I EPR transition results from a positive hf coupling, the high-frequency ENDOR lines from three negative hf couplings. As expected from Fig. 3A, the positions of the ENDOR lines with respect to ν_H are exchanged, when the Z_{II} EPR transition connecting the $m_S=0$ and $m_S=-1$ levels is selected (Fig. 3B). Now the line of the positive hf coupling is shifted to higher frequency and those of the negative hf couplings to lower frequency. The ENDOR spectrum connected to the Z_{II} EPR transition is, as expected from Fig. 3A, in emission, but has been inverted in Fig. 3B for better comparison. The obtained hf couplings $A_Z(i)$ are given in Table 1.

A comparison of the pulse ENDOR spectrum for the EPR Z_I transition of ^{3}P680 and the triplet state of chlorophyll in MTHF, ^{3}Chl a, is given in the lowest two traces of Fig. 4. Note that the frequency scale gives here the deviation from ν_H. For ^{3}P680 only one narrow line is observed on the low-frequency side corresponding to one positive $A_Z(1)$, but three lines are observed on the high-frequency side, corresponding to three negative $A_Z(2,3,4)$ values. Due to the high triplet yield and strong spin polarisation (selective population of the $m_S=0$ level), it was possible to set the EPR field at the outer wing of the Z_I edge (Fig. 2B), resulting in a very narrow orientation selection. The spectrum of ^{3}Chl a exhibits broader lines as compared with ^{3}P680. This has probably two reasons. (i) ^{3}Chl a is generated by spin orbit-induced intersystem crossing from the excited singlet state of Chl a, with a lower triplet yield and less selective population of the triplet sublevels as compared with ^{3}P680. Consequently the signals were much smaller as for ^{3}P680. Therefore, spectra with sufficient signal-to-noise ratio could not be obtained at the outer wings of the Z_I edge, and an EPR field setting close to the maximum of the Z_I edge had to be chosen, resulting in a broader distribution of orientations contributing to the ENDOR spectrum. (ii) For ^{3}Chl a in frozen glassy organic solution (MTHF), a distribution of slightly different microenvironments is expected, which results in a distribution of the ZFS parameters D and E (ZFS-strain), as well as in a distribution of the hf-tensor values $A_{X,Y,Z}$, which both causes broadening of the observed ENDOR lines.

For ^{3}Chl a one intense line is observed on the low-frequency side (positive $A_Z(1)$). In addition there is a weak broad shoulder near -5 MHz, which is not observed in

Table 1
Hyperfine couplings [MHz] for the methyl and methine protons of ^{3}P680, ^{3}Chl *a*, and the cation and anion radical states Chl $a^{+\bullet}$ and Chl $a^{-\bullet}$

Molecule[a]	Hyperfine component[b]	Assignment[c]					
		12 (1)	2	7	5 (2)	10 (3)	20 (4)
^{3}P680	A_X	+11.4	nd	nd	−7.1	−4.7	−3.3
	A_Y	+10.0	nd	nd	−1.8	−14.8	−11.8
	A_Z	+9.5	nd	nd	−5.5	−10.4	−8.4
	A_{iso}	+10.3	nd	nd	−4.8	−10.0	−7.8
^{3}Chl *a*	A_Z	+7.4	nd	nd	(−6.2)	−11.4	−7.2
Chl $a^{+\bullet}$[d]	A_{iso}	+7.12	+3.04	+3.04	≤ |0.6|	≤ |0.6|	≤ |0.6|
Chl $a^{-\bullet}$[e]	A_{iso}	+10.58	+5.34	−1.53	−4.67	−11.68	−4.37

[a] See molecular structure, Fig. 5.
[b] Principal component of the respective hyperfine tensor, axes collinear with the ZFS axes *X*, *Y*, *Z*. A_Z-tensor values of +9.6 and −5.4 MHz for ^{3}P680 and +8.7 MHz for ^{3}Chl *a* have been reported in Ref. [33].
[c] See text, Fig. 5 for molecular positions and Fig. 4 for line numbering (in brackets) nd, not determined.
[d] ENDOR in liquid solution, radical generated with I_2 in CH_2Cl_2. A_{iso} = +10.3 and +10.1 MHz for β-protons at positions 17 and 18, see text [9,47].
[e] ENDOR in liquid solution, radical generated electrolytically in 1,2-dimethoxy-ethane (DME). A_{iso} = +1.7 and −1.53 MHz for β-protons at positions 17 and 18, see text [9,48].

^{3}P680 (see below). Only two lines are clearly resolved on the high-frequency side, A_Z(3,4). However, a weak third line, A_Z(2), seems to be superimposed on the low-frequency side of the line at −7 MHz or, alternatively, on the low-frequency side of the line at 10–11 MHz. The obtained hf tensor components A_Z(i) are listed in Table 1.

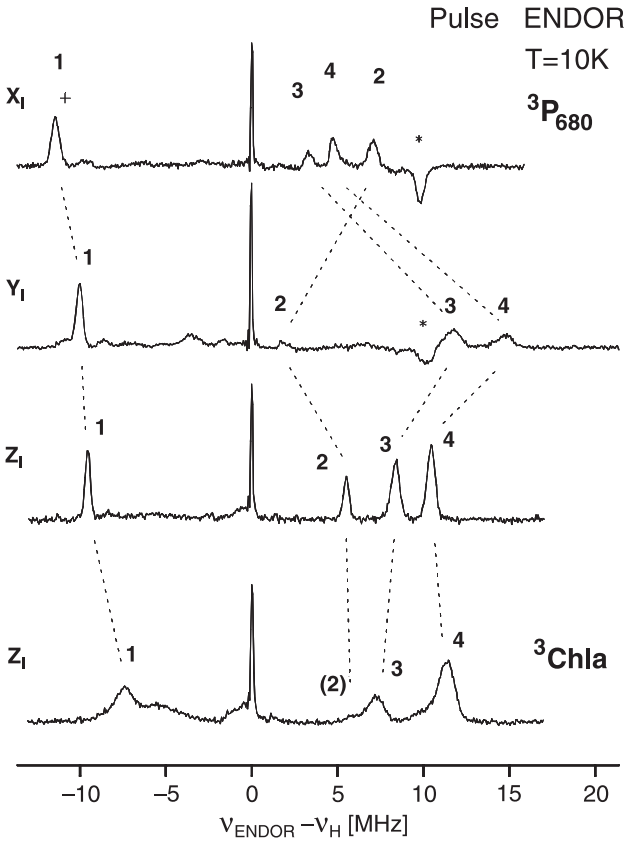

Fig. 4. Pulse ENDOR spectra of ^{3}P680 for the three EPR field positions X_I, Y_I, and Z_I (compare Fig. 2). Lowest trace: Pulse ENDOR spectrum for ^{3}Chl *a* for the Z_I EPR field position. For experimental conditions see text. Each trace accumulated for ≈ 15 h at *T* = 10 K. The frequency scale gives the deviation from ν_H in the respective spectra (narrow intense line) for better comparison. The hyperfine values $A_{X,Y,Z}$(i) correspond to the frequency shift between ν_H and the respective ENDOR line (see text).

There is only one previous study reporting hf values A_Z(i) from ^{3}P680 and ^{3}Chl *a* [33]. In that work a different technique, transient ENDOR, was used, which is more sensitive to smaller couplings. Several small hf couplings were observed in Ref. [33], which are difficult to observe with pulse ENDOR used in the present study. Also some of the large couplings have been observed by these authors (see Table 1, caption). The two A_Z(i) values reported for ^{3}P680 agree within the error margins with the A_Z(1) and A_Z(2) values of our study. The two larger negative values A_Z(3,4) found in our work were, however, not reported in Ref. [33]. The positive A_Z(1) value observed in the previous study for ^{3}Chl *a* [33] is somewhat larger than the value in this paper. This could be due to the different solvent used. None of the negative A_Z(2,3,4) values were observed in Ref. [33]. The data presented in Table 1 represent the first complete set of the large hf couplings for ^{3}P680 and ^{3}Chl *a*, which reflect the major spin densities in the HOMO and LUMO orbitals of the respective triplet state.

3.2.2. ENDOR spectra from the X_I and Y_I orientations of ^{3}P680

Pulse ENDOR spectra of ^{3}P680 were also measured for the other canonical orientations where the magnetic field B_0 is parallel to the zero field axes *X* and *Y* (EPR transitions X_I and Y_I). The obtained ENDOR spectra for these EPR transitions are shown in Fig. 4, upper two traces. For the X_I spectrum three high-frequency lines 2, 3, 4, resulting from negative A_X(2,3,4) values, are observed, which are significantly shifted to lower frequencies as compared with the spectrum for the Z_I EPR transition. There is also a small shift of the low-frequency line 1, resulting from a positive A_X(1) value. Interestingly there is an additional inverted line (in emission) on the high-frequency side at ≈ 10 MHz. Closer inspection of Fig. 2B shows that the X_I position in the EPR

spectrum corresponds to an edge of the powder pattern of the absorptive $m_S = 0$ to $m_S = +1$ transition, and hence good orientation selection along X is achieved for the ENDOR lines connected with this EPR transition, which are expected to be in absorption (compare Fig. 3A). This is reflected in the narrow lines of the ENDOR spectrum. However, at the X_I position in the EPR spectrum (Fig. 2B) there is also a contribution expected from the emissive $m_S = 0$ to $m_S = -1$ transitions, from orientations in the Z–Y and Z–X plane not too far from Z_{II}. The ENDOR lines connected to this EPR transition are expected to be in emission. Indeed, an emissive line, marked with an asterisk, is observed on the high-frequency side in the X_I ENDOR spectrum (Fig. 4). Since for this "Z_{II}" transition the high- and low-frequency ENDOR lines are exchanged (see Fig. 3B) this line should correspond to the positive coupling $A_Z(1)$. The value of the hf coupling from this line agrees remarkably well with the $A_Z(1)$ value observed in the Z_I and Z_{II} spectra. The emissive high-frequency ENDOR line in the X_I ENDOR spectrum is surprisingly narrow in view of the fact that the emissive EPR part at the X_I EPR field position does not correspond to a canonical orientation but to a distribution of noncanonical orientations both in the Z–Y and Z–X plane (Fig. 2B). This is due to the small anisotropy of the A(1) hf tensor which leads only to small shifts of the ENDOR line 1 in the X_I, Y_I, and Z_I ENDOR spectra. Similar emissive ENDOR lines from $m_S = 0$ to $m_S = -1$ EPR transitions are also expected from the negative hf couplings of lines 2, 3, and 4. These should appear on the low-frequency side of the X_I ENDOR spectrum. The corresponding hf tensors A(2,3,4) have, however, much larger anisotropy (see below), which broadens these emissive lines on the low-frequency side beyond detection.

The Y_I field position (Fig. 4, trace 2) is expected to pick up not only the Y-orientation, but also a distribution of orientations, both from the $m_S = 0$ to $m_S = +1$ and the $m_S = 0$ to $m_S = -1$ transitions. Consequently the observed lines from anisotropic couplings are broader than those obtained at the other orientations. Two of the three high-frequency lines corresponding to negative $A_Y(3,4)$-values are shifted to considerably higher frequencies. The third line, from $A_Y(2)$, has very low intensity and is shifted close to ν_H (see discussion below). Again there is an additional emissive line marked with an asterisk on the high-frequency side resulting from the positive coupling from the $m_S = 0$ to $m_S = -1$ EPR transition (Fig. 2B). The low-frequency line at ≈ -10 MHz (positive $A_Y(1)$) is still narrow and close to its position in the Z_I spectrum. Several very weak additional features are observed on the low-frequency side (see below).

It is obvious from Fig. 4 that the negative hf couplings exhibit a large anisotropy, while the anisotropy for the positive hf coupling is small. This explains why in the X_I- and Y_I-spectra the emissive lines from the $m_S = 0$ to $m_S = -1$ EPR transition, which are observed for the positive hf coupling A(1), are not observed for the negative hf tensors A(2,3,4). All anisotropic hf tensor components obtained, $A_{X,Y,Z}$(i), are collected in Table 1.

For the in vitro triplet ^{3}Chl a, no pulse ENDOR spectra were recorded from the X_I- and Y_I-orientations. This was a consequence of the lower triplet yield and much lower spin polarisation for ^{3}Chl a, which is generated by spin–orbit-coupling-induced intersystem crossing (see above). In particular for the X_I- and X_{II}-orientation only very small signal intensities were observed already in the pulse EPR spectra (data not shown), making it impossible to obtain pulse ENDOR spectra for these orientations. However, we expect the anisotropy of the respective hf tensors for ^{3}Chl a to be similar to those determined for ^{3}P680, since both triplet states originate from monomeric chlorophyll species. We also note that a sound comparison of the spin density distribution of both triplet states is obtained already from the pulse ENDOR spectra for the Z_I- and Z_{II}-orientations (see above). The triplet Z-axis is perpendicular to the molecular plane in both cases, and is therefore the same molecular axis in both chlorophyll species. Furthermore, this axis is expected to be also a principal axis of the observed hf tensors for the CH_3 and methine protons in both triplet states. Hence, changes of the spin density distribution of ^{3}Chl a and ^{3}P680 should be directly reflected in the hf values A_Z(i) for the respective nuclei (i).

4. Discussion

4.1. Assignment of hf tensor components of ^{3}P680 and ^{3}Chl a

For the triplet state in bacterial RCs, we have shown previously that an assignment of the observed hf tensors to specific nuclei can be achieved by comparing the components A_Z(i) with the isotropic hf coupling constants from the respective cation and anion radicals [18,47–49]. This is justified by the following reasons. (i) For an α-proton, directly attached to a carbon atom of the π-system, this tensor component is expected to be close to the isotropic value $A_{iso} = 1/3(A_x + A_y + A_z)$. The calculated values for an isolated C–H fragment are $0.5 \times A_{iso}$, $1.5 \times A_{iso}$, and $1 \times A_{iso}$, for the A_x-, A_y- and A_z-tensor components, respectively, with z being parallel to the p_Z-orbital of the carbon carrying a π-spin density and x being parallel to the C–H bond and perpendicular to z (note that in Fig. 5 the indices in $A_{X,Y,Z}$ indicate the directions of the ZFS tensor, which agree with this definition only for positions 10 and 20. For position 5 A_X and A_Y are exchanged with respect to this definition). A_{iso} scales with the π-spin density and has a value of -60 MHz for a spin density of 1 [49]. Hence, A_Z should be always close to A_{iso}. For β-protons, which are one bond away from the π-system, in particular for those from rotating methyl groups, only a small anisotropy of about 10% of A_{iso} is expected, i.e. the tensor values are close to A_{iso}. Hence, for both types of protons the A_Z(i) values should be close to the respective A_{iso} values. (ii) In the simple Hückel approximation, the hf coupling for a given nucleus of a triplet state is expected to be the average of

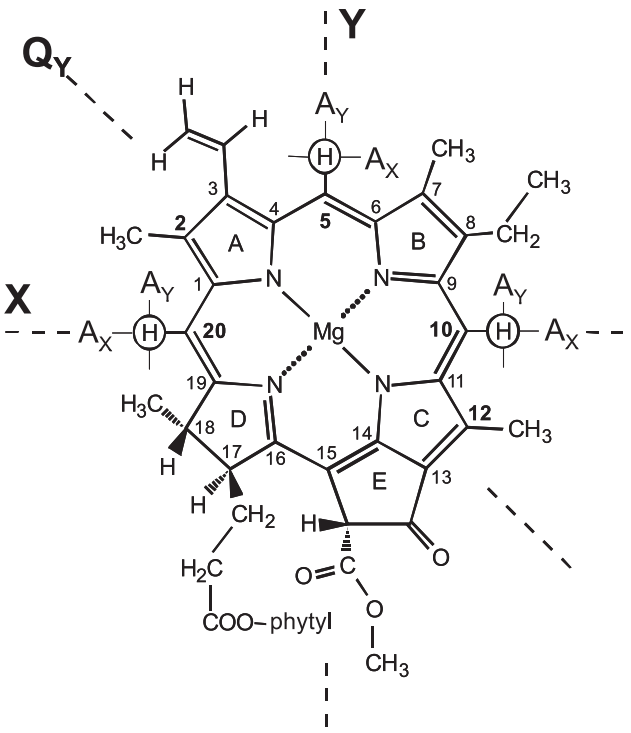

Fig. 5. Molecular structure of Chl *a* with numbering scheme. Orientation of the Q_Y transition dipole axis from Ref. [58]. The orientations of the ZFS tensor (*X* and *Y*) and the hyperfine tensors of protons at positions 5, 10, and 20 (A_X and A_Y) were obtained from the ENDOR data (see text). *Z*-axis is perpendicular to the molecular plane.

that observed in the respective cation (singly occupied HOMO) and anion radical (singly occupied LUMO), $(A(^3P) = 1/2[(A(P^{+\bullet}) + A(P^{-\bullet})]$ [49] because in the triplet state both orbitals, the HOMO and LUMO are singly occupied. This approximation gives a rough qualitative picture of the expected hf values, which reflect the unpaired spin density distribution.

Table 1 lists the major isotropic hf coupling constants of Chl $a^{+\bullet}$ and Chl $a^{-\bullet}$ obtained from previous work [47,48]. In the cation radical all larger couplings have positive values and result from the CH_3 protons at positions 2, 7, and 12, and from the β-protons 17 and 18 of ring D (see Fig. 5 and Table 1). In the anion radical, on the other hand, large negative couplings are observed for the methine protons 5, 10, and 20, but also large positive values for the CH_3 protons 2 and 12. Therefore, the negative A_Z(i)-values in the triplet states are assigned to the methine protons. They result from unpaired spin density in the LUMO orbital [18]. Based on its small anisotropy the positive coupling $A_Z(1)$ is assigned to protons of a rotating methyl group.

From comparison with the Chl $a^{+\bullet}$ and Chl $a^{-\bullet}$ data, it is unexpected that only one narrow line corresponding to one positive $A_Z(1)$-value is observed in ^{3}P680. However, the same effect, only one positive hf coupling, was observed earlier for the bacterial triplet states, ^{3}BChl *a*, in organic solvent, and ^{3}P865 in bacterial RCs [18]. Both CH_3 groups at positions 2 and 12 (Fig. 5) exhibit reasonably large hf couplings in the cation and anion radical. The coupling from the CH_3 group at positions 2 is smaller than that from position 12, in particular in the cation radical (Table 1). Hence, two different couplings would be expected from these two methyl groups in the triplet state. A possible explanation for the missing ENDOR line of the protons from the methyl group at position 2 could be that this group shows a restricted rotation at the low temperature used ($T = 10$ K), probably due to steric effects caused by the neighbouring vinyl group (Fig. 5). Rotation of CH_3 groups is known to be a major source of nuclear (proton) spin relaxation at low temperature [50]. Small nuclear relaxation rates could prevent reestablishment of equilibrium populations between the laser pulses, thereby diminishing the ENDOR amplitudes. Similar effects of weak and broadened ENDOR lines from methyl protons at low temperatures have been reported earlier for bacteriochlorophyll cation radicals [51]. The coupling of the third CH_3 group in Chl *a* at position 7 exhibits in the cation radical a small positive value, and is in the anion radical close to zero. Consequently only a small coupling would be expected for the triplet state. We therefore assign A(1) in ^{3}P680 to the CH_3 group at position 12. This is in line with the relative magnitudes of the hf-tensor components $A_{X,Y,Z}(1)$. The largest value $A_X(1)$ is expected for the C–CH_3 bond direction, which is consistent with an assignment to position 12, but not consistent with an assignment to position 7 (see below).

It should be noted that the used Davies pulse ENDOR technique is sensitive for large hf couplings, but less sensitive for very small couplings, and ENDOR line intensities from transitions in the $m_S = +1$ and $m_S = -1$ manifolds decrease as they approach the Zeeman frequency ν_H. This is a consequence of the band width of the first microwave π-pulse, which does not allow selective excitation of EPR transitions, which are separated by hf couplings smaller than this band width (Fig. 3A, and Ref. [44]). This effect is reflected in the intensity pattern of the high-frequency lines in the Z_I spectrum (Fig. 3B). This, however, does not hold for the ENDOR transition in the $m_S = 0$ manifold, which occurs at ν_H and is very narrow because it experiences no hf shift (Fig. 3A). Small hf couplings can be detected by other pulse ENDOR techniques like Mims-ENDOR [44]. Such additional experiments were not performed in view of the extended accumulation times (≈ 15 h) necessary for recording one ENDOR spectrum. Furthermore, several small hf couplings for ^{3}P680 have been reported in an earlier paper [33]. The goal of this investigation was to obtain all of the large hf couplings, which reflect the majority of the spin density distribution.

Interestingly a broad weak feature at ≈ −5 to −6 MHz corresponding to one or more additional positive hf couplings is observed in the Z_I spectrum of ^{3}Chl *a* (Fig. 4). Such a structure is not observed in the Z_I spectrum of ^{3}P680. However, the Y_I spectrum of ^{3}P680 shows a few weak features at about −8 to −6 MHz. These could correspond to the "missing" hf couplings from the CH_3 group at position

2, and/or from the β-protons at 17 and 18 (Fig. 5 and Table 1, caption). The low intensity of these signals, however, is not understood. It could be due to slow relaxation rates for these β-protons as referred to above for ^{3}P680. These features may be more pronounced in ^{3}Chl *a* than in ^{3}P680 due to a broader distribution of orientations contributing to the Z_I-ENDOR spectrum of ^{3}Chl *a* (see below). Due to their weak intensities these features are not further discussed in this paper. Their corresponding hf values would, however, fit into the general picture of the strong hf couplings, since they have comparable magnitude in ^{3}Chl *a* and ^{3}P680.

The obtained absolute values of the couplings, $|A_Z(\mathrm{i})|$, in particular those of the negative couplings, are significantly larger than the expected average of the cation and anion value of Chl *a* (Table 1). This behaviour was observed already earlier for the triplet states in the bacterial RC, ^{3}P865, and for ^{3}BChl *a* [18]. Apparently, there is a considerable redistribution of spin densities in the triplet state orbitals, both for the chlorophyll molecules in organic solvent and in the RCs, as compared with the respective cation and anion orbitals, leading to high spin densities with LUMO character on the methine positions. This observation urges for theoretical calculations on a more sophisticated quantum chemical level, which, to our knowledge, were so far not performed on these chlorophyll triplet states.

4.2. Comparison of ^{3}P680 and ^{3}Chl a

It is obvious from Fig. 4 and from Table 1 that the respective A_Z(i)-values of ^{3}P680 and ^{3}Chl *a* show a fairly good agreement. This is in contrast to the bacterial RC, where the couplings in ^{3}P865 were significantly decreased by more than a factor of 2 and the respective lines were split as compared with ^{3}BChl *a* [18]. This clearly indicated an asymmetric delocalisation over two BChla molecules. For the plant PS II triplet state, ^{3}P680, investigated here, the positive coupling changes from 7.4 MHz in ^{3}Chl *a* to an even larger value of 9.5 MHz in ^{3}P680. The two larger negative couplings, -7.8 and -10.0 MHz, of ^{3}P680 are close to the respective values of ^{3}Chl *a*. The line of the third negative coupling, $A_Z(2)$, is not clearly resolved in the spectrum of ^{3}Chl *a*, however, there is a weak low-frequency shoulder with a corresponding $A_Z(2)$-value of -6.2 MHz on the $A_Z(3)$-line at 7 MHz (Fig. 4). Alternatively, the third line may be hidden under the weak shoulder of the $A_Z(4)$-line at 10–11 MHz. The sum of these three negative couplings is remarkably similar for ^{3}Chl *a* and ^{3}P680 in the case of the former assignment.

Comparison with the respective A_Z(i)-values of ^{3}Chl *a* corroborates the view obtained from comparison of the *D*- and *E*-values that at low temperature (T= 10 K), ^{3}P680 is a monomeric ^{3}Chl *a* species in the PS II complexes investigated here. It also shows that there are small shifts of the individual A_Z(i)-values, which we attribute to specific interactions with the protein, e.g. hydrogen bonding to the 13^1 carbonyl group (Fig. 5). MTHF used as solvent for ^{3}Chl *a* is not expected to form hydrogen bonds. Hydrogen bonding to this keto group is known to enhance the hf coupling of the adjacent CH_3 group at position 12 in the cation radical [52]. Previous transient EPR studies on ^{3}P680 by other authors indicated a possible delocalisation at higher temperatures [53,54]. Pulse ENDOR experiments, which we tried at higher temperature, were, however, not successful because of a sharp decrease of signal intensity at elevated temperatures.

4.3. Assignment of the ZFS- and hf-tensor axes in the Chl a molecular frame

The EPR field settings X_I, Y_I, and Z_I (Fig. 2B) correspond to orientations, where the respective axes of the ZFS tensor, *X*, *Y*, and *Z*, are parallel to the magnetic field. Hence, evaluation of the respective ENDOR spectra should give information on the relative orientations of the hf tensor axes and the ZFS axis system. For the α-protons at the methine positions, strongly anisotropic hf tensors are expected with the smallest tensor component ($0.5 \times A_{iso}$) along the C–H bond, the largest component ($1.5 \times A_{iso}$) in the molecular plane, perpendicular to the C–H bond, and the third intermediate component ($1 \times A_{iso}$) perpendicular to the plane (see above).

The *Z*-axis of the ZFS tensor of a π–π* triplet state like a chlorophyll molecule is perpendicular to the molecular π-plane [45]. Therefore, the Z_I and Z_{II} ENDOR spectra originate from molecules oriented with their molecular planes perpendicular to the magnetic field. This corresponds to a principal orientation of the hf tensor of the methine protons, A_Z, which is reflected in the narrow lines observed in the ENDOR spectra (Fig. 4). The hf components A_Z(i) obtained (Table 1) are thus a principal value of the tensor for the respective methine proton.

For the other orientations, X_I and Y_I, the situation is less obvious. The X_I position corresponds to an edge of the powder pattern of the absorptive $m_S = 0$ to $m_S = +1$ transition and hence to a good orientation selection of the triplet molecule along the *X* axis. But it is not obvious whether this orientation corresponds to a principal axis of the methine proton hf-tensor. Closer inspection of the high-frequency ENDOR lines of the methine proton lines of the X_I and Z_I spectra shows that they have the same line width of $\approx$ 0.5 MHz. An estimate of the orientation distribution selected for the X_I spectrum indicates that angular deviations from $\pm 5°$ up to $\pm 10°$ from the ZFS tensor *X*-axis contribute to the X_I ENDOR spectrum. In this case much larger line widths, up to 2 MHz, are estimated from the respective $A_X(3,4)$ and $A_Y(3,4)$ values in the case of significantly deviating hf- and ZFS-axes systems. We therefore conclude that the orientation selected for X_I is close to a principal axis orientation for all three methine protons, 5, 10, 20, within approximately $\pm 10°$.

The Y_I ENDOR spectrum (Fig. 4) is expected to pick up intensities from a distribution of orientations both from the absorptive and the emissive EPR transitions (Fig. 2B).

Hence, anisotropic broadening is expected in this ENDOR spectrum. Nevertheless, two well-resolved absorptive lines from methine protons are observed on the high-frequency side at about 12 and 15 MHz, which are approximately 50% broader as compared with the Z_I and X_I spectra. It has been observed in previous transient EPR and pulse EPR studies on porphyrin triplet states that anisotropic electronic T_2 relaxation time gives rise to intensity patterns in the pulse-EPR spectra, which deviate from those calculated for equal contributions from all orientations. In particular, the intensities along the ZFS principal axes were enhanced as compared with other orientations [55]. The field-swept electron spin echo (ESE) spectrum of ^{3}P680 (Fig. 2C) clearly shows such reduced signal intensities for noncanonical orientations. This effect was explained by shorter T_2 relaxation times for orientations between the ZFS principal axes, which is induced by modulation of the ZFS axes orientations. These modulations are expected to have largest amplitudes for orientations, where the angular dependence of the ZFS is strong (45° off from the ZFS axes), and small amplitudes along the ZFS axes orientations. This effect is apparent also in the ENDOR spectra that were recorded as radio-frequency-dependent changes of the EPR echo amplitude (see above, and Fig. 1). Hence, the lines in the Y_I ENDOR spectrum represent the enhanced contributions from the principal components A_Y(i) of the respective hf tensors.

Thus the ENDOR spectra indicate that the hf tensor axes of the methine protons are parallel to the ZFS tensor axes. The hf tensor axes of these protons are directly related to the respective bond directions and hence the orientation of the ZFS axes *X*, *Y*, *Z* was obtained as shown in Fig. 5. This orientation is in good agreement with the results from an earlier optical study on ^{3}Chl *a* where linear dichroic triplet-minus-singlet difference spectra were recorded, and an angle of $\pm 48°$ was obtained between *X* and the transition dipole moment vector for the optical Q_Y transition [56,57]. The orientation of Q_Y, shown in Fig. 5, was determined earlier by optical work on pyro-chlorophyllide in myoglobin single crystals [58]. However, in the optical study [56,57] only the angles between the Q_Y- and *X*-, *Y*-axes were obtained, leaving two possible orientations of the ZFS axes with respect to the molecular axes, i.e. the *X*- and *Y*-axes shown in Fig. 5 could be exchanged (the angles were close to 45°). Our data remove this ambiguity and yield the unique assignment shown in Fig. 5. For each of the methine protons the largest in-plane hf tensor component is expected perpendicular to the C–H bond, the smallest component parallel to the C–H bond. Two large negative couplings, A_Y(3,4), are observed in the ENDOR spectrum along Y_I (high-frequency lines, Fig. 4), which we therefore assign to the two methine protons with collinear tensors at positions 10 and 20. Hence, the *Y*-direction, along which the ENDOR spectrum was obtained, must be perpendicular to these C–H bonds as shown in Fig. 5. The smallest tensor components, A_X(3,4), of these protons are assigned to the two smaller negative couplings from the X_I ENDOR spectrum (Fig. 4 and Table 1). For the proton at position 5, assigned to line 2, the relative magnitudes of A_X(2) and A_Y(2) are expected to be exchanged. Its largest in-plane value perpendicular to its C–H bond is expected along *X* and assigned to the largest negative value from the ENDOR spectrum along X_I. Its smallest component is expected along *Y* and is assigned to the smallest negative coupling resulting from the weak line on the high-frequency side close to ν_H, as indicated in the Y_I ENDOR spectrum. With this assignment all three methine protons exhibit relative amplitudes of their hf components $A_{X,Y,Z}$ (2,3,4) as expected for C–H groups being attached to a π-system (see above and Ref. [49].

This assignment is also consistent with the anisotropy observed for the positive hf tensor A(1), assigned to the CH_3 protons at position 12. The largest values for a rotating CH_3 group are expected along the C–CH_3 bond, which is almost parallel to *X* for the CH_3 groups at positions 2 and 12; see Fig. 5. The perpendicular orientation in the plane (*Y*) and the out-of plane orientation (*Z*) are expected to have both similar values, which should be smaller than that for *X*. This is indeed observed (compare the low-frequency sides of the *X*-, *Y*- and *Z*-ENDOR spectra in Fig. 4; for values see Table 1). This behaviour of the hf-tensor components $A_{X,Y,Z}$(1) further corroborates the assignment to the methyl group at positions 12 (or 2) and not to position 7 (see above).

5. Conclusion

In this work, time-resolved pulse ENDOR combined with repetitive laser excitation at cryogenic temperature was used to obtain the hf structure from the short-lived triplet states ^{3}P680 in plant photosystem II and ^{3}Chl *a* in a frozen organic solvent. The data obtained represent the first complete set of the larger hf tensor values from all three canonical orientations for ^{3}P680 and from the *Z*-orientation for ^{3}Chl *a*. They indicate a redistribution of spin densities, in particular in the LUMO orbitals of ^{3}Chl *a* and ^{3}P680, as compared with the cation and anion radicals from Chl *a*. This deviation of the triplet state hf couplings from those expected from comparison with the cation and anion radicals is not understood at present and is a challenge for future theoretical studies on these triplet states using advanced quantum chemical methods.

Comparison of the hf data for ^{3}Chl *a* and ^{3}P680 clearly confirms that ^{3}P680 is a monomeric Chl *a* species at low temperature ($T = 10$ K), as has been proposed earlier based on *D*- and *E*-values obtained from EPR and ODMR studies [8,14,15,20]. Beyond that, shifts of the hf couplings of individual nuclei were observed, which are of particular interest since they indicate specific protein interactions, e.g. hydrogen bonding to the keto group in ring E.

The ENDOR spectra, obtained here for the in-plane *X*- and *Y*-orientations of the ZFS tensor, enabled a full determination of the hf tensors of the three methine protons and one CH_3 group of ^{3}P680. Based on the orientations of these

hf tensor axes, the orientations of the in-plane axes of the ZFS tensor were determined. They were found to agree well with previously reported angles between the electronic Q_Y transition dipole and the ZFS *X*- and *Y*-axes, obtained from optical experiments [56,57]. In the present work a unique determination of the orientations of the ZFS tensor axes, *X* and *Y*, of ^{3}P680 in the Chl *a* molecular axis system was achieved, which was not possible in earlier studies, where *X*- and *Y*-axes in Fig. 5 could be exchanged. This result is a prerequisite for obtaining the molecular orientation of ^{3}P680 in the PS II protein structure from EPR studies on PS II single crystals (M. Kammel et al., this issue [37]).

The spin (and electron) distribution obtained for the LUMO orbital of ^{3}P680 is of particular interest, since light-induced electron transfer starts from this orbital in the excited singlet state of the primary donor. However, for PS II the identity and nature of the primary donor is still under debate. Recently models have been discussed, which involve Chl_{D1} as primary donor before the positive charge moves to one of the two Chl molecules (P_{D1} and P_{D2}) called "P680" [38,40,59,60]. The EPR experiments on ^{3}P680 in oriented membrane fragments [36] and on ^{3}P680 in PS II single crystals [37] demonstrate that this triplet state may indeed reside on one of the two accessory chlorophylls, Chl_{D1} or Chl_{D2}. In this model, ^{3}P680 may reside indeed on the same molecule, which acts as very early primary electron donor. The small but significant shifts of hf values of ^{3}P680 as compared with those of ^{3}Chl *a* are most probably induced by specific interactions with the protein, e.g. hydrogen bonding, which could be further investigated by pulse ENDOR on ^{3}Chl *a* using different solvents, which form hydrogen bonds, e.g. to the 13^1 keto group (Fig. 5). In this way, it may be possible in future studies to use site-directed mutagenesis to assign the triplet state, ^{3}P680, specifically to one of the two chlorophyll molecules, Chl_{D1} and Chl_{D2}, in the photosystem II structure.

Acknowledgements

This work was supported by Deutsche Forschungsgemeinschaft (SFB 498, TP C5), European Union (FMRX-CT98-0214) and Fonds der Chemischen Industrie (WL). AT received two travel Fellowships from the European Science Foundation. The biochemical isolations were carried out by AT in the laboratory of Prof J. Barber, Imperial College, with support from the Biotechnology and Biological Sciences Research Council.

References

[1] Govindjee (Series Ed.), Advances in Photosynthesis, vols. 1–11, Kluwer Academic Publishing, Dordrecht, 1995–2001.
[2] P. Jordan, P. Fromme, H.T. Witt, O. Klukas, W. Saenger, N. Krauß, Three-dimensional structure of cyanobacterial photosystem I at 2.5 Å resolution, Nature 411 (2001) 909–917.
[3] R.E. Blankenship, M.T. Madigan, C.E. Bauer, Anoxygenic photosynthetic bacteria, in: C.E. Govindjee (Ed.), Advances in Photosynthesis, vol. 2, Kluwer Academic Publishing, Dordrecht, 1995.
[4] D.R. Ort, C.F. Yocum, Oxygenic photosynthesis: the light reactions, in: C.F. Govindjee (Ed.), Advances in Photosynthesis, vol. 4, Kluwer Academic Publishing, Dordrecht, 1996.
[5] A. Zouni, H.T. Witt, J. Kern, P. Fromme, N. Krauß, W. Saenger, P. Ort, Crystal struture of photosystem II from *Synechococcus elongatus*, Nature 409 (2001) 739–743.
[6] C.R.C. Lancaster, U. Ermler, H. Michel, The structures of photosynthetic reaction centers from purple bacteria as revealed by X-ray crystallography, in: R.E. Blankenship, M.T. Madigan, C.E. Bauer (Eds.), Anoxyggenic Photosynthetic Bacteria, in: Govindjee (Series Ed.), Advances in Photosynthesis, vol. 2, Kluwer Academic Publishing, Dordrecht, 1995, pp. 503–526.
[7] A.J. Hoff, Applications of ESR in photosynthesis, Phys. Rep. 54 (1979) 84–200.
[8] A.J. Hoff, J. Deisenhofer, Photophysics of photosynthesis, Phys. Rep. 287 (1997) 1–247.
[9] W. Lubitz, EPR and ENDOR studies of chlorophyll cation and anion radicals, in: H. Scheer (Ed.), Chlorophylls, CRC Press, Boca Raton, FL, 1991, pp. 903–944.
[10] J. Amesz, A.J. Hoff (Eds.), Biophysical Techniques in Photosynthesis, in: Govindjee (Ed.), Advances in Photosynthesis, vol. 3, Kluwer Academic Publishing, Dordrecht, 1996, pp. 209–313, Chap. 13–18.
[11] W. Lubitz, F. Lendzian, R. Bittl, Radicals, radical pairs and triplet states in photosynthesis, Acc. Chem. Res. 35 (2002) 313–320.
[12] R.J. Cogdell, T.D. Howard, R. Bittl, E. Schlodder, I. Geisenheimer, W. Lubitz, How carotenoids protect bacterial photosynthesis, Philos. Trans. R. Soc. Lond., B 355 (2000) 1345–1349.
[13] A.J. Hoff, Optically detected magnetic resonance (ODMR) of triplet states in photosynthesis, Biophysical techniques in photosynthesis, in: Govindjee (Series Ed.), Advances in Photosynthesis, vol. 3, Kluwer Academic Publishing, Dordrecht, 1996, pp. 277–298.
[14] D.E. Budil, M.C. Thurnauer, The chlorophyll triplet state as a probe of structure and function in photosynthesis, Biochim. Biophys. Acta 1057 (1991) 1–41.
[15] R. Bittl, E. Schlodder, I. Geisenheimer, W. Lubitz, R.J. Cogdell, Transient EPR and absorption studies of carotenoid triplet formation in purple bacterial antenna complexes, J. Phys. Chem., B 105 (2001) 5525–5535.
[16] A. deWinter, S.G. Boxer, The mechanism of triplet energy transfer from the special pair to the carotenoid in bacterial photosynthetic reaction centers, J. Phys. Chem., B 103 (1999) 8786–8789.
[17] J. Barber, B. Andersson, Too much of a good thing—light can be bad for photosynthesis, Trends Biochem. Sci. 17 (1992) 61–66.
[18] F. Lendzian, R. Bittl, W. Lubitz, Pulsed ENDOR of the photo-excited triplet states of bacteriochlorophyll a and of the primary donor P865 in reaction centers of *Rhodobacter sphaeroides* R-26, Photosynth. Res. 55 (1998) 189–197.
[19] H. Levanon, J.R. Norris, The photoexcited triplet state and photosynthesis, Chem. Rev. 78 (1978) 185–198.
[20] J.R. Norris, D.E. Budil, P. Gast, C.-H. Chang, O. El-Kabbani, M. Schiffer, Correlation of paramagnetic states and molecular structure in bacterial photosynthetic reaction centers: The symmetry of the primary electron donor in *Rhodopseudomonas viridis* and *Rhodobacter sphaeroides* R-26, Proc. Natl. Acad. Sci. U. S. A. 86 (1989) 4335–4339.
[21] M.C. Thurnauer, ESR study of the photoexcited triplet state in photosynthetic bacteria, Rev. Chem. Intermed. 3 (1979) 197–230.
[22] F. Lendzian, M. Huber, R.A. Isaacson, B. Endeward, M. Plato, B. Bönigk, K. Möbius, W. Lubitz, G. Feher, The electronic structure of the primary donor cation radical in *Rhodobacter sphaeroides* R-26: ENDOR and TRIPLE resonance studies in single crystals of reaction centers, Biochim. Biophys. Acta 1183 (1993) 139–160.
[23] A.N. Webber, W. Lubitz, P700: the primary electron donor of photosystem I, Biochim. Biophys. Acta 1507 (2001) 61–79.

[24] H. Käß, P. Fromme, H.T. Witt, W. Lubitz, Orientation and electronic structure of the primary donor radical cation $P_{700}^{+\cdot}$ in photosystem I. A single crystals EPR and ENDOR study, J. Phys. Chem., B 105 (2001) 1225–1239.
[25] H. Käß, E. Bittersmann-Weidlich, L.-E. Andréasson, B. Bönigk, W. Lubitz, ENDOR and ESEEM of the ^{15}N labelled radical cations of chlorophyll *a* and the primary donor P_{700} in photosystem I, Chem. Phys. 194 (1995) 419–432.
[26] S.E.J. Rigby, J.H.A. Nugent, P.J. O'Malley, ENDOR and special triple resonance studies of chlorophyll cation radicals in photosystem 2, Biochemistry 33 (1994) 10043–10050.
[27] A. Telfer, F. Lendzian, J. Barber, W. Lubitz, ENDOR and transient absorption studies of $P_{680}^{+\cdot}$ and other cation radicals in PS II reaction centers before and after inactivation of secondary electron donors, in: G. Garab (Ed.), Photosynthesis, Mechanisms and Effects, vol. II, Kluwer Academic Publishing, Dordrecht, 1998, pp. 1057–1060.
[28] N.W. Woodbury, J.P. Allen, The pathway, kinetics and thermodynamics of electron transfer in wild type and mutant reaction centers of purple nonsulfur bacteria, in: R.E. Blankenship, M.T. Madigan, C.E. Bauer (Eds.), Anoxygenic Photosynthetic Bacteria, in: Govindjee (Series Ed.), Advances in Photosynthesis, vol. 2, Kluwer Academic Publishing, Dordrecht, 1995, pp. 527–557.
[29] H. van Amerongen, L. Valkunas, R. van Grondelle, Photosynthetic Excitons, World Scientific Publishing, Singapore, 2000.
[30] T. Förster, Delocalized excitation and excitation transfer, in: O. Sinanoglu (Ed.), Modern Quantum Chemistry, vol. IIIB, Academic Press, New York, 1965, pp. 93–137.
[31] D.L. Dexter, A theory of sensitized luminescence in solids, J. Chem. Phys. 21 (1953) 836–850.
[32] F. Lendzian, F.H. van Willigen, S. Sastry, K. Möbius, H. Scheer, R. Feick, Proton ENDOR study of the photoexcited triplet state P^T in *Rps. sphaeroides* R-26 photosynthetic reaction centers, Chem. Phys. Lett. 118 (1985) 145–150.
[33] M. Di Valentin, C.W.M. Kay, G. Giacometti, K. Möbius, A time-resolved electron-nuclear double resonance study of the photoexcited triplet state of P680 in isolated reaction centers of photosystem II, Chem. Phys. Lett. 248 (1996) 434–441.
[34] J. Hanley, Y. Deligiannakis, A. Pascal, P. Faller, A.W. Rutherford, Carotenoid oxidation in photosystem II, Biochemistry 38 (1999) 8189–8195.
[35] P. Faller, T. Maly, A.W. Rutherford, F. MacMillan, Chlorophyll and carotenoid radicals in photosystem II studied by pulsed ENDOR, Biochemistry 40 (2001) 320–326.
[36] F.J.E. van Mieghem, K. Satoh, A.W. Rutherford, A chlorophyll tilted 30° relative to the membrane in the photosystem II reaction centre, Biochim. Biophys. Acta 1058 (1991) 379–385.
[37] M. Kammel, J. Kern, W. Lubitz, R. Bittl, Photosystem II single crystals studied by transient EPR: the light-induced triplet state, Biochim. Biophys. Acta 1605 (2003) 47–54 (this issue).
[38] B.A. Diner, E. Schlodder, P.J. Nixon, W.J. Coleman, F. Rappaport, J. Lavergne, W.F.J. Vermaas, D.A. Chisholm, Site-directed mutations at D1-His198 and D2-His197 of photosystem II in *Synechocystis* PCC 6803: Sites of primary charge separation and cation and triplet stabilization, Biochemistry 40 (2001) 9265–9281.
[39] B.A. Diner, F. Rappaport, Structure, dynamics, and energetics of the primary photochemistry of photosystem II of oxygenic photosynthesis, Annu. Rev. Plant Biol. 53 (2002) 551–580.
[40] V.O. Prokhorenko, A.R. Holzwarth, Primary processes and structure of the photosystem II reaction center: a photon echo study, J. Phys. Chem., B. 104 (2000) 11563–11578.
[41] J. De Las Rivas, A. Telfer, J. Barber, 2-Coupled β-carotene molecules protect P680 from photodamage in isolated photosystem-II reaction centers, Biochim. Biophys. Acta 1142 (1993) 155–164.
[42] F. Lendzian, R. Bittl, A. Telfer, J. Barber, W. Lubitz, Time resolved ENDOR of the triplet state of P680 in PS II reaction centers, in: G. Garab (Ed.), Photosynthesis: Mechanisms and Effects, vol. II, Kluwer Academic Publishing, Dordrecht, 1998, pp. 1057–1060.
[43] D. Stehlik, K. Möbius, New EPR methods for investigating photoprocesses with paramagnetic intermediates, Annu. Rev. Phys. Chem. 48 1997, pp. 745–784.
[44] A. Schweiger, Pulsed electron spin resonance: basic principles and applications, Angew. Chem., Int. Ed. Engl. 30 (1991) 265–292;
A. Schweiger, G. Jeschke, Principles of Pulse Electron Paramagnetic Resonance, Oxford Univ. Press, Oxford, 2001.
[45] J.A. Kooter, J.H. van der Waals, Metastable triplet-state of zinc porphin and magnesium porphin—study by ESR in an *n*-octane crystal at 1.4 K, Mol. Phys. 37 (1979) 997–1013.
[46] N.M. Atherton, Principles of Electron Spin Resonance, Ellis Horwood PTR Prentice Hall, New York, 1993.
[47] M. Huber, F. Lendzian, W. Lubitz, E. Tränkle, K. Möbius, M.R. Wasielewski, ENDOR and triple resonance in solutions of the chlorophyll *a* and bis(chlorophyll)cyclophane radical cations, Chem. Phys. Lett. 132 (1986) 467–473.
[48] A.J. Hoff, F. Lendzian, K. Möbius, W. Lubitz, Proton and nitrogen electron nuclear double and triple resonance of the chlorophyll *a* anion in liquid solution, Chem. Phys. Lett. 85 (1982) 3–8.
[49] A. Carrington, A.D. McLachlan, Introduction to Magnetic Resonance with Applications to Chemistry and Chemical Physics, Harper & Row, New York, 1969.
[50] M. Brustolon, A.L. Maniero, M. Bonora, U. Segre, Electron spin relaxation times and internal motions of radicals in the solid state investigated by ENDOR and pulsed EPR, Appl. Magn. Reson. 11 (1996) 99–113.
[51] G. Feher, A.J. Hoff, R.A. Isaacson, L.C. Ackerson, ENDOR experiments on chlorophyll and bacteriochlorophyll in vitro and in the photosynthetic unit, Ann. N.Y. Acad. Sci. 244 (1975) 239–259.
[52] H. Käß, W. Lubitz, G. Hartwig, H. Scheer, D. Noy, A. Scherz, ENDOR studies of substituted chlorophyll cation radicals, Spectrochim. Acta 54A (1998) 1141–1156.
[53] I. Sieckmann, K. Brettel, C. Bock, A. van der Est, D. Stehlik, Transient electron paramagnetic resonance of the triplet state of P700 in photosystem I: evidence for triplet delocalization at room temperature, Biochemistry 32 (1993) 4842–4847.
[54] A. Kamlowski, L. Frankemöller, A. van der Est, D. Stehlik, Evidence for delocalization of the triplet state $^3P680$ in the $D_1D_2cytb_{559}$-complex of photosystem II, Ber. Bunsenges. Phys. Chem. 100 (1996) 2045–2051.
[55] C.W.M. Kay, G. Elger, K. Möbius, The photoexcited triplet state of free-base porphycene: a time-resolved EPR and electron spin echo investigation, Phys. Chem. Chem. Phys. 1 (1999) 3999–4002.
[56] J. Vrieze, P. Gast, A.J. Hoff, Structure of the reaction center of photosystem I of plants. An investigation with linear-dichroic absorbance-detected magnetic resonance, J. Phys. Chem. 100 (1996) 9960–9967.
[57] J. Vrieze, Optical and magnetic properties of chlorophylls in glasses and in photosynthetic pigment–protein complexes, PhD thesis, University of Leiden, The Netherlands, 1994.
[58] R.S. Moog, A. Kuki, M.D. Fayer, S.G. Boxer, Excitation transport and trapping in synthetic chlorophyllide substituted hemoglobin: orientation of the chlorophyll S1 transition dipole, Biochemistry 23 (1984) 1564.
[59] J. Dekker, R. van Grondelle, Primary charge separation in Photosystem II, Photosynth. Res. 63 (2000) 195–208.
[60] T. Noguchi, Dual role of triplet localization on the accessory chlorophyll in the photosystem II reaction center: photoprotection and photodamage of the D1 protein, Plant Cell Physiol. 43 (2002) 1112–1116.